High Charge-Carrier Mobility in π-Deficient Discotic Mesogens: Design and Structure–Property Relationship

Matthias Lehmann,*[a, d] Gaël Kestemont,[a] Rafael Gómez Aspe,[a] Claudine Buess-Herman,[c] Michel H. J. Koch,[e] Michael G. Debije,[f] Jorge Piris,[f] Matthijs P. de Haas,[f] John M. Warman,[f] Mark D. Watson,[g] Vincent Lemaur,[h] Jérôme Cornil,[h] Yves Henri Geerts,*[a] Raluca Gearba,[b] and Dimitri A. Ivanov[b]

Abstract: Hexaazatrinaphthylene (HATNA) derivatives with six alkylsulfanyl chains of different length (hexyl, octyl, decyl and dodecyl) have been designed to obtain new potential electron-carrier materials. The electron-deficient nature of these compounds has been demonstrated by cyclic voltammetry. Their thermotropic behaviour has been studied by means of differential scanning calorimetry and polarised optical microscopy. The supramolecular organisation of these discotic molecules has been explored by temperature-dependent X-ray diffraction on powders and oriented samples. In addition to various liquid crystalline columnar phases (Col_{hd}, Col_{rd}), an anisotropic plastic crystal phase is demonstrated to exist. The charge-carrier mobilities have been measured with the pulse-radiolysis time-resolved microwave-conductivity technique. They are found to be higher in the crystalline than in the liquid crystalline phases, with maximum values of approximately 0.9 and 0.3 $cm^2 V^{-1} s^{-1}$, respectively, for the decylsulfanyl derivative. Mobilities strongly depend on the nature of the side chains.

Keywords: charge-carrier mobility · columnar mesophases · electron-deficient mesogens · liquid crystals · X-ray diffraction

Introduction

During the last decade, increasing attention has been paid to discotic aromatic compounds that form columnar liquid crystals because the overlap of π orbitals results in one-dimensional semiconductors with a better performance than conjugated polymers. Discotic liquid crystals have already found applications as active components in organic light-

[a] Dr. M. Lehmann, G. Kestemont, Dr. R. Gómez Aspe, Prof. Y. H. Geerts
Laboratoire de Chimie des Polymères, CP 206/1, Université Libre de Bruxelles
Boulevard du Triomphe, 1050 Bruxelles (Belgium)
E-mail: matthias.lehmann@chemie.tu-chemnitz.de
ygeerts@ulb.ac.be

[b] R. Gearba, Prof. D. A. Ivanov
Laboratoire de Physique des Polymères, CP 223, Université Libre de Bruxelles
Boulevard du Triomphe, 1050 Bruxelles (Belgium)

[c] Prof. C. Buess-Herman
Laboratoire de Chimie Analytique et Chimie des Interfaces, CP 255, Université Libre de Bruxelles
Boulevard du Triomphe, 1050 Bruxelles (Belgium)
Fax: (+32) 2-650-5410

[d] Dr. M. Lehmann
Current address: Non-Classical Synthetic Methods
Institute of Chemistry, Chemnitz University of Technology
Strasse der Nationen 62, 09111 Chemnitz (Germany)
Fax: (+49) 371-531-1839

[e] Dr. M. H. J. Koch
European Molecular Biology Laboratory, EMBL c/o DESY
Notkestrasse 85, 22603 Hamburg (Germany)

[f] Dr. M. G. Debije, Dr. J. Piris, Dr. M. P. de Haas, Dr. J. M. Warman
IRI, Delft University of Technology
Mekelweg 15, 2629 JB Delft (The Netherlands)

[g] Dr. M. D. Watson
Max Planck Institute for Polymer Research
Ackermannweg 10, 55128, Mainz (Germany)
current address: Department of Chemistry, University of Kentucky, Lexington, KY 40506–0055 (USA)

[h] V. Lemaur, Dr. J. Cornil
Laboratory for Chemistry of Novel Materials
Center for Research on Molecular Electronics and Photonics, Université de Mons-Hainaut
Place du Parc, 20, 7000 Mons (Belgium)

Supporting information for this article is available on the WWW under http://www.chemeurj.org/ or from the author.

 DOI: 10.1002/chem.200400586 © 2005 Wiley-VCH Verlag GmbH & Co. KGaA, Weinheim

emitting diodes,[1,2] photovoltaic cells[1,3] and field effect transistors.[1,4] Common features that impact on the device performance are charge injection or collection at the electrodes and charge transport in the bulk material. The latter depends on the degree of order within the columnar stack and thus on the overlap between the π-orbitals. Charge-carrier mobilities of $0.1\,cm^2V^{-1}s^{-1}$ have been measured for hexahexylsulfanyltriphenylene[5] in its highly ordered helical columnar H-phase, and even higher mobilities, up to $0.5\,cm^2V^{-1}s^{-1}$, have been recorded for liquid crystalline hexabenzocoronene derivatives.[6] These electron-rich mesogens are *p*-type semiconductors,[7] thus promoting efficient hole transport. Although many aromatic discotic mesogens are known today, only few of them show *n*-type semiconducting properties.[8] The lack of efficient organic electron transporters originates from various factors: 1) the high reactivity of radical anions with impurities, such as water and oxygen,[9,10] 2) the low energy of the lowest unoccupied molecular orbital (LUMO), which should be close to the work function of the metal used as the anode for electron injection, and 3) the generally smaller electronic splitting of the LUMO level compared to the highest occupied molecular orbital (HOMO), which is a measure of the charge-transfer efficiency between adjacent aromatic cores in the columns.[11] Most of the existing columnar electron carriers are designed by substitution of aromatic CH groups of the core by nitrogen atoms,[12] lateral substitution with electron-withdrawing groups, such as carboxyl groups,[13] amides and imides,[14,15] or by combining the two principles,[15] that is, by the use of nitrogen-containing aromatic cores with electron-withdrawing substituents. For all these discotic mesogens, attempts have only been made to increase the electron-deficient nature of their aromatic cores. Little attention has been devoted to the optimisation of the parameters favouring the migration of electrons down the stack by a hopping mechanism where charges jump from disk to disk to yield a current. The most relevant parameters have been described by recent quantum-chemical calculations within the framework of the Marcus theory and correspond to: 1) the LUMO splitting corresponding to twice the transfer integral t for electrons, and 2) the internal reorganisation energy λ, associated with the geometric distortions induced by the hopping to go from the neutral state to the radical anion (λ_1) for one molecule and from the radical anion to the neutral state (λ_2) for the other molecule.[11,16] The amplitude of λ and t dictates the hopping frequency. A large hopping rate, and hence a high mobility, requires small values for λ and large values for t. An attempt to take account of the mentioned requirements in the design of an electron-carrier material has been made by the synthesis of new electron-deficient hexaazatrinaphthylene derivatives **1** (Scheme 1), which have been recently reported by our group.[17] Six alkylsulfanyl chains were laterally attached to the core in order to obtain columnar liquid crystalline phases and to increase the solubility in common solvents. The mesomorphism has been shown to depend strongly on the chain length, which has been increased from hexyl, to octyl, to decyl and finally to dodecyl chains. Preliminary examinations of the surface potential decay on drop-cast, non-oriented samples of **1** suggest that both negative and positive charges are mobile in the material.[7] In the present work, we will elaborate on the design principles for molecules **1** and will demonstrate their electron-deficient nature by means of cyclic voltammetry. The phases were identified by polarised optical microscopy (POM), differential scanning calorimetry (DSC) and X-ray diffraction. The latter was carried out on powder samples during consecutive heating and cooling cycles and is complemented by diffraction patterns on extruded fibres, obtained

Abstract in French: *L'hexaazatrinaphthylène substitué par six chaînes alkylsulfanyls forme potentiellement de nouveaux matériaux transporteurs d'électrons. Ces molécules ont été synthétisées avec différentes longueurs de chaînes alkyl: hexyl, octyl, decyl et dodecyl. La nature électrodéficiente est démontrée par voltampérométrie cyclique. Le comportement thermotrope de ces matériaux a été étudié par calorimétrie différentiel à balayage et par microscopie optique à lumière polarisée. La dépendance en température de l'organisation supramoléculaire des molécules discotiques a été explorée au moyen de la diffusion de rayons X sur des échantillons en poudre et orientés. En plus des différentes phases cristal liquides des colonnes (Col_{hd}, Col_{rd}), l'existence d'une phase cristal plastique anisotrope est démontrée. La mobilité des porteurs de charge a été mesurée par la méthode de "pulse-radiolysis time-resolved microwave conductivity". Les mobilités sont plus élevées pour les phases cristallines que pour les phases cristal liquides avec, respectivement, des valeurs maximum proches de 0.9 et $0.3\,cm^2V^{-1}s^{-1}$ pour la molécule avec des chaînes decylsulfanyls. Les mobilités dépendent fortement de la nature des chaînes latérales.*

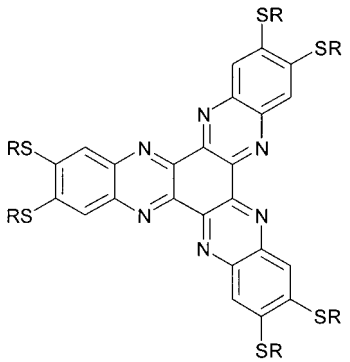

1a : SR = S-C_6H_{13}

1b : SR = S-C_8H_{17}

1c : SR = S-$C_{10}H_{21}$

1d : SR = S-$C_{12}H_{25}$

Scheme 1. Hexaazatrinaphthylene **1** derivatives as electron-deficient mesogens.

 © 2005 Wiley-VCH Verlag GmbH & Co. KGaA, Weinheim

at selected temperatures, at which distinct mesophases are present. The structural data are then related to the charge-carrier mobilities measured by the pulse-radiolysis time-resolved microwave conductivity (PR-TRMC) technique.

Results and Discussion

Molecular design: The molecular design of compounds **1** was based on several requirements: 1) The π-conjugated core should be electron deficient to ease electron injection or collection at the electrode and to stabilise the radical anion (negative polaron) with respect to reactions with water or oxygen. 2) The shape of the LUMO orbital should lead to a favourable overlap between adjacent disks within the columns, and thus to a large transfer integral t. Moreover, the orbital overlap should be rather insensitive to the rotational and translational disorder characteristic of columnar stacks. 3) The molecular structure should exhibit low reorganisation energy λ. 4) The attachment of flexible chains should induce liquid crystal (LC) behaviour by microsegregation of the rigid aromatic core and the flexible aliphatic chains, and lead to self-healing columnar assemblies with high intracolumnar order, that is, a regular, preferably coplanar stacking of aromatic cores with small interdisk distance. 5) The synthesis should deliver the target molecules by a short and efficient route and with high purity.

Molecule **1** has been designed based on the above-mentioned requirements. The LUMO level has been lowered in energy by the incorporation of six nitrogen atoms into the central core. Six sulfur atoms have also been attached to the periphery of the aromatic system since they are known to stabilise radical anions.[18] The favourable orbital overlap is achieved by the fact that the six carbon atoms of the central ring as well as the six nitrogen atoms have the same sign in the LCAO pattern (Figure 1); as a result, the rotation does not introduce a mixing between bonding and antibonding overlaps and hence does not lead to vanishingly small splittings, as illustrated in Figure 1. The molecules should also display a small internal reorganisation energy λ during the hopping process. Reorganisation energies have been recently discussed for various aromatic cores.[19] The following trends have been derived: 1) λ decreases with increasing core size, 2) sulfur at the periphery is preferred over oxygen, and 3) introduction of nitrogen atoms into the aromatic core leads to an increase of λ. A reorganisation energy of 0.11 eV has been calculated for negative polarons (radical anions) in **1** with six SH groups,[19] which is rather low and comparable to the reorganisation energy calculated for positive polarons in a large and efficient hole carrier, such as hexabenzocoronene (HBC). For the sake of comparison, we emphasise that the reorganisation energy for negative polarons amounts to 0.24 eV for a triphenylene molecule substituted by six SH groups.

As already mentioned, LC behaviour is generally induced by attachment of flexible chains to the rigid core. A series of saturated chains of different lengths ranging from hexylsulfanyl to dodecylsulfanyl have been linked to the periphery of **1** in order to systematically study the LC behaviour and phase structures of the disks because the supramolecular self-assembly of mesogens can not be accurately predicted as yet. Furthermore, aliphatic chains also increase the solubility and hence the processability of the molecules from solution. Finally, electron-carrier mesogen **1** can be synthesised by an efficient two-step synthesis, which facilitates structural variation of the side-chains and preparation of the material on the multi-gram scale.[17] All compounds have been exhaustively purified by chromatography and crystallisation procedures (see the Experimental Section).

Cyclic voltammetry: The investigation of the π-deficient character and the stabilisation of radical anions of **1a** has been carried out by cyclic voltammetry. The electrochemical features of these derivatives were probed at room temperature (RT) in a dichloromethane solution versus the standard calomel electrode (SCE) with a glassy carbon electrode at a scan rate of 200 mV s^{-1}. It has been found that these molecules show three reduction waves centred at approximately −1.09, −1.35 and −1.60 V (Figure 2), which probably arise from the formation of the corresponding mono-, di- and tri-radical anions. No oxidation waves have been observed below +2 V, highlighting the mainly reducible nature of these compounds. With respect to the nature of the reduction processes when recorded at different scan rates, one could expect a relatively long lifetime for the radical anion species. This can be accounted for by the ability of the alkylthio lateral groups to stabilise radical anions.[18] Despite the tendency of these large discotic mesogens to stack in solution to form aggregates,[17] no remarkable

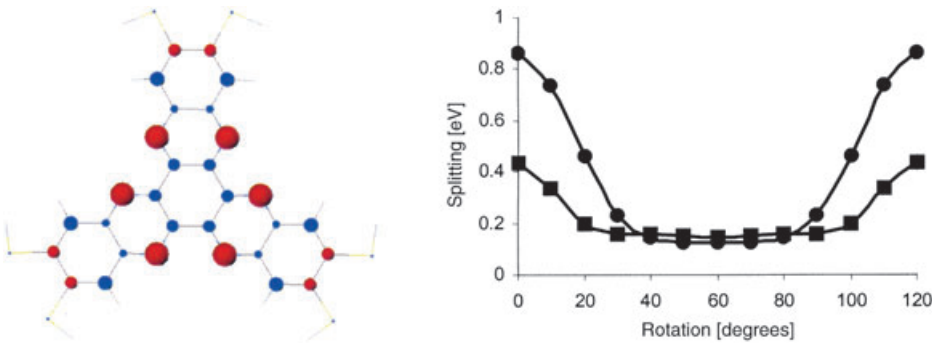

Figure 1. Left: shape of the LUMO orbital of HATNASH; the colour and the size of the balls correspond to the sign and the amplitude of the LCAO coefficients, respectively. Right: INDO-calculated evolution of the HOMO (●) and LUMO (■) splittings in a cofacial dimer consisting of two HATNA molecules as a function of the rotational angle between the disks.

 © 2005 Wiley-VCH Verlag GmbH & Co. KGaA, Weinheim

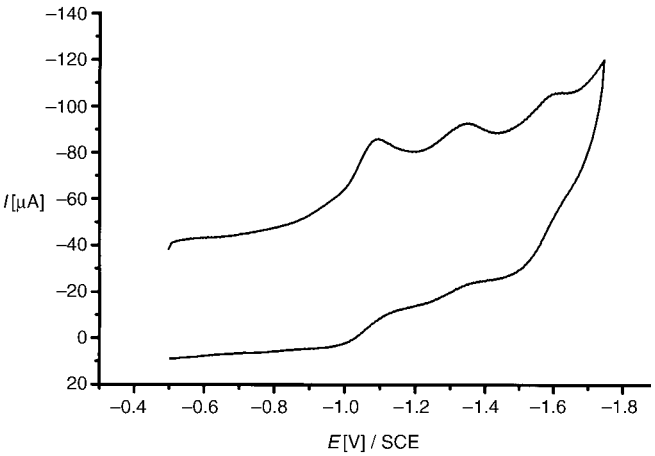

Figure 2. Cyclic voltammogram of HATNA derivative **1a** in CH_2Cl_2 (10^{-3} mol L^{-1}) at a scan rate of 200 mV s^{-1}.

changes were observed in their electrochemical behaviour over a range of concentrations in dichloromethane (10^{-3}–10^{-4} mol L^{-1}). However, even in this concentration range and under the conditions of the cyclic voltammetric measurements, aggregates are present as evidenced by ^{1}H NMR studies (see the Supporting Information). Consequently, the electron affinity (EA) and the LUMO energy level cannot be estimated according to the equation EA = (E_{red} + 4.75)[20] for a single molecule. Owing to the low reduction potential of −1.09 V, it is anticipated that electrons can be easily injected in these disklike molecules and that these compounds could be good candidates for applications as electron conducting layers in electronic devices. In such devices, traces of water and oxygen will strongly influence the electron transport, thus *n*-type material of satisfactory stability would be desirable. A stability window versus water and oxygen for semiconducting materials has been defined by de Leeuw et al.[9] According to their work, *n*-type doped semiconductors are stable with respect to water if the oxidation potential of the radical anion is higher than −0.66 V (SCE), and stable with respect to oxygen if it is higher than +0.57 V (SCE). The hexaazatrinaphthalene derivatives **1** with a first reduction wave at −1.09 V are out of this window and presumably will only be useful in water- and oxygen-free electronic devices.

Differential scanning calorimetry and polarised optical microscopy: Table 1 summarises the data on the thermotropic behaviour of the studied compounds. The structure assignment of the LC phases is based on X-ray data presented in detail below. As previously emphasised,[17] compounds **1a–d** show a complex polymorphism, especially for molecules with intermediate chain lengths. Some transitions at high temperature (**1c**,**d**) are not apparent in the DSC thermograms, and can only be identified by X-ray diffraction. Such a behaviour has already been observed for other discotic mesogens, such as tetrabenzocyclodecatetraene.[21] Note that compounds **1a–d** begin to decompose at approximately 250 °C before clearing into an isotropic phase. Therefore, the samples were not heated above 230 °C. The inability of cooling from the isotropic phase prevents the observation of characteristic textures in polarised optical microscopy (POM). However, all phases referred to as mesophases exhibit two inherent properties of liquid crystalline material: birefringence and fluidity. Uniform, unspecific textures could be only obtained when the material was oriented by shearing in the hexagonal phase; upon cooling to the lower transitions, very small domains were again formed, which could not be attributed to a typical texture. At all lower transitions passed during cooling of **1**, no significant changes of the texture could be observed. Up to five consecutive heating and cooling cycles were performed in DSC. The reproducibility of the transition data demonstrates the reversibility of the LC transitions and the stability of the material from room temperature to 230 °C.

The simplest phase behaviour was obtained for **1a**. After purification of the crude material, a mixture of crystalline phases is observed, as revealed by two endothermic transitions at 155 °C and 205 °C. Upon heating above 205 °C, the material forms a fluid LC phase. Subsequent cooling and heating cycles lead only to the more stable crystalline phase (Cr_1), which melts at 206 °C, and the high-temperature mesophase. For the other molecules **1b–d**, the crystals formed

Table 1. Thermotropic behaviour of mesogens **1** studied by means of differential scanning calorimetry (DSC) at a heating rate of 10 °C min^{-1}.

Compound	DSC trace	Phase transitions, transition temperature (onset) [°C]/transition enthalpy [kJ mol^{-1}][a]
1a	1st heating	Cr_0[c] 155/10.0 Cr_1 205/23.7 Col_{hd}
	1st cooling	Col_{hd} 196/−26.5 Cr_1
	2nd heating	Cr_1 206/26.4 Col_{hd}
1b	1st heating	Cr_0 148/39.5 Cr_1 175/13.6 Col_{hd}
	1st cooling	Col_{hd} 174/−12.5 Cr_1 43/−7.6 Cr_2
	2nd heating	Cr_2 77/5.6 Cr_3 –/–[e] Cr_4 142/14.0 Cr_1 178/13.5 Col_{hd}
1c[d]	1st heating	Cr_0[c] 95/112 Cr_1 113/10 X/Col_{rd0} 134/1.0 Col_{rd1} 181/0.2 Col_{rd2} 222/– Col_{hd}
	1st cooling	Col_{hd} –/–[b] Col_{rd2} 181/−0.3 Col_{rd1} 128/−1.8 Col_{rd0}/X 95/−3.7 Cr_2 17/−28.1 Cr_3
	2nd heating	Cr_3 26/4.5 Cr_4 40/18.4 Cr_5 50/−24.1 Cr_1 116/30.6 X 134/1.6 Col_{rd1} 180/0.4 Col_{rd2} –/–[b] Col_{hd}
1d[d]	1st heating	Cr_0 90/134 Col_{rd} 149/–[b] Col_{hd}
	1st cooling	Col_{hd} 147/–[b] Col_{rd} 79/−32.4 Cr_1
	2nd heating	Cr_1 99/31.7 Col_{rd} 149/–[b] Col_{hd}

[a] The crystal phases Cr_x have been numbered in the order of their appearance during the heating and cooling cycles. [b] The transition to the hexagonal phase has been detected in X-ray measurements during the first heating phase. [c] In the first heating phase (after synthesis), a mixture of different crystal modifications is obtained. However, there is one dominant structure, as shown by X-ray studies. [d] The transition to the hexagonal columnar phase has only been observed by X-ray diffraction. [e] Slow crystallisation is observed after the endothermic transition at 77 °C.

© 2005 Wiley-VCH Verlag GmbH & Co. KGaA, Weinheim

during the purification procedures (Cr_0) differed from the crystal phases obtained after the first heating cycle (Cr_1), a result not only evident from X-ray data (vide infra), but also by comparison of transition temperatures and enthalpies corresponding to the first heating and subsequent cooling and heating traces: melting and crystallisation enthalpies and temperatures show large deviations, thus indicating that the transitions are not reversible. During the second heating phase, compound **1b** exhibits a low-temperature crystal phase (Cr_2). After complex melting and crystallisation processes (Cr_3, Cr_4), followed by a high-temperature modification (Cr_1), the material transforms into a LC phase at 178 °C.

The most complex polymorphism is found for **1c**. The metastable Cr_0 melts at 95 °C and partially forms a Cr_1 phase, which melts at 113 °C, followed by the formation of various mesophases. In the DSC trace, two transitions with very small enthalpies were observed during heating and cooling above the melting temperature of Cr_1. The phase between 115–134 °C is waxy and assigned as an X phase, which could be an anisotropic plastic crystal.[22] On cooling the X phase, a relatively small enthalpy (-3.7 kJ mol^{-1}) is measured for the transition to the crystal (Cr_2) at 95 °C and a further crystallisation is observed below room temperature. The subsequent heating trace exhibits two endothermic signals at 26 °C and 40 °C. The material then exhibits crystallisation on heating at 50 °C to yield the Cr_1 phase, which melts again at 116 °C to assemble in the mesophase. Because the small transition enthalpy in the cooling trace at 95 °C is rather unusual for a crystallisation, and owing to the large enthalpy difference between crystallisation X/Cr_2 (-3.7 kJ mol^{-1}) and melting Cr_1/X (30.6 kJ mol^{-1}), the temperature range between 70 and 120 °C has been investigated in more detail (for DSC traces see the Supporting Information). When directly heated after cooling to 70 °C, the material shows only a relatively small enthalpy change of 17.3 kJ mol^{-1} on transforming into the X phase. In addition to the transition at 116 °C, a shoulder with an onset at 112 °C is visible, which is attributed to the Cr_2/X transition. After annealing the sample at 70 °C for 30 min, the heating trace exhibits only a large transition at 116 °C (36.1 kJ mol^{-1}). Thus, on cooling the X phase, a crystal phase Cr_2 forms, which is metastable and slowly transforms into the more stable Cr_1 phase. The crystalline character of Cr_2 is supported by its rigidity in POM studies and its large thermal hysteresis of 17 °C. The small enthalpic change (X/Cr_2) suggests that the plastic X phase and the metastable Cr_2 phase do not have large structural differences.

Compound **1d** displays an even simpler thermotropic behaviour. In the first heating phase, a large endothermic peak is associated with the melting of the Cr_0 phase. Further cooling and heating traces show relatively smaller transition enthalpies for the single transition observed close to 100 °C. Although the material looks pasty, the large hysteresis of 20 °C and a relatively large transition enthalpy of approximately 32 kJ mol^{-1} suggest the existence of a crystalline phase at low temperature. Above the melting temperature, only one LC phase is determined by DSC. However, temperature-dependent X-ray powder diffraction reveals the formation of a second LC phase above 149 °C, as discussed below.

X-ray diffraction

*Powder X-ray diffraction of compound **1d***: We will first focus on compound **1d**, which yields the most instructive X-ray results. Figure 3a and 3b show the DSC curves, and the corresponding temperature-dependent powder X-ray patterns, respectively, of **1d**. The first X-ray diffractogram (A) (Figure 3b) of the as-prepared sample was recorded at room temperature before the first heating phase. The material is clearly in a crystalline phase (Cr_0), although the indexation could not be unambiguously established.[23] However, at wide angles the large reflection at $d = 3.85$ Å and the somewhat weaker reflection at 3.73 Å are reminiscent of the 110 and 200 peaks typically found for HDPE.[24] The less intense reflection at 3.5 Å, which is a typical intermolecular distance in π stacks,[25,26] could be associated with the regular organisation of the aromatic cores. The second pattern (B) was also recorded at low temperature, but after completion of the first heating and cooling cycle. The original structure (Cr_0) is not recovered on cooling and the absence of a sharp peak in the wide angular range provides evidence that a regular π-stacking of aromatic cores is not present in this phase. The X-ray results for the LC phases forming above the melting point at 99 °C are shown in the following five diffraction patterns reported in Figure 3b (C–G). The wide-angle region of all patterns consists of only a broad halo, which can be attributed to the average distance between the liquid-like aliphatic side chains. The absence of mixed reflections *hkl* demonstrates the disappearance of positional long-range order of the 3D lattice, and consequently, the formation of a LC phase. In contrast to the invariance of the scattering at wide angles, the small-angle region shows considerable temperature dependence. The structure of the low-temperature mesophase was analyzed using diffractogram C, recorded just before the LC/Cr transition when cooling the material to 100 °C. The X-ray pattern shows a series of five reflections which can be indexed according to a primitive rectangular unit cell ($a = 46.6$, $b = 27.6$ Å; two-dimensional lattice type *p2gg*; see Table 2 and Figure 5C). In the second heating trace, the 120 and 410 reflections disappear at high temperature. The size of the unit cell slightly expands, as indicated by a shift of the remaining reflections to smaller *s* values, corresponding to larger Bragg distances. At 149 °C, the 210 reflection, which determines the rectangular symmetry of the two-dimensional lattice, vanishes and only two reflections, whose reciprocal spacing follows the ratio $1:\sqrt{3}$ persist. Therefore, the columnar mesophase is hexagonal (Col_h) above this temperature. This transition, which was not observed during DSC measurements, was reproduced by X-ray diffraction at the same temperature in the second heating phase, thus excluding a degradation effect by heat or radiation.

 © 2005 Wiley-VCH Verlag GmbH & Co. KGaA, Weinheim

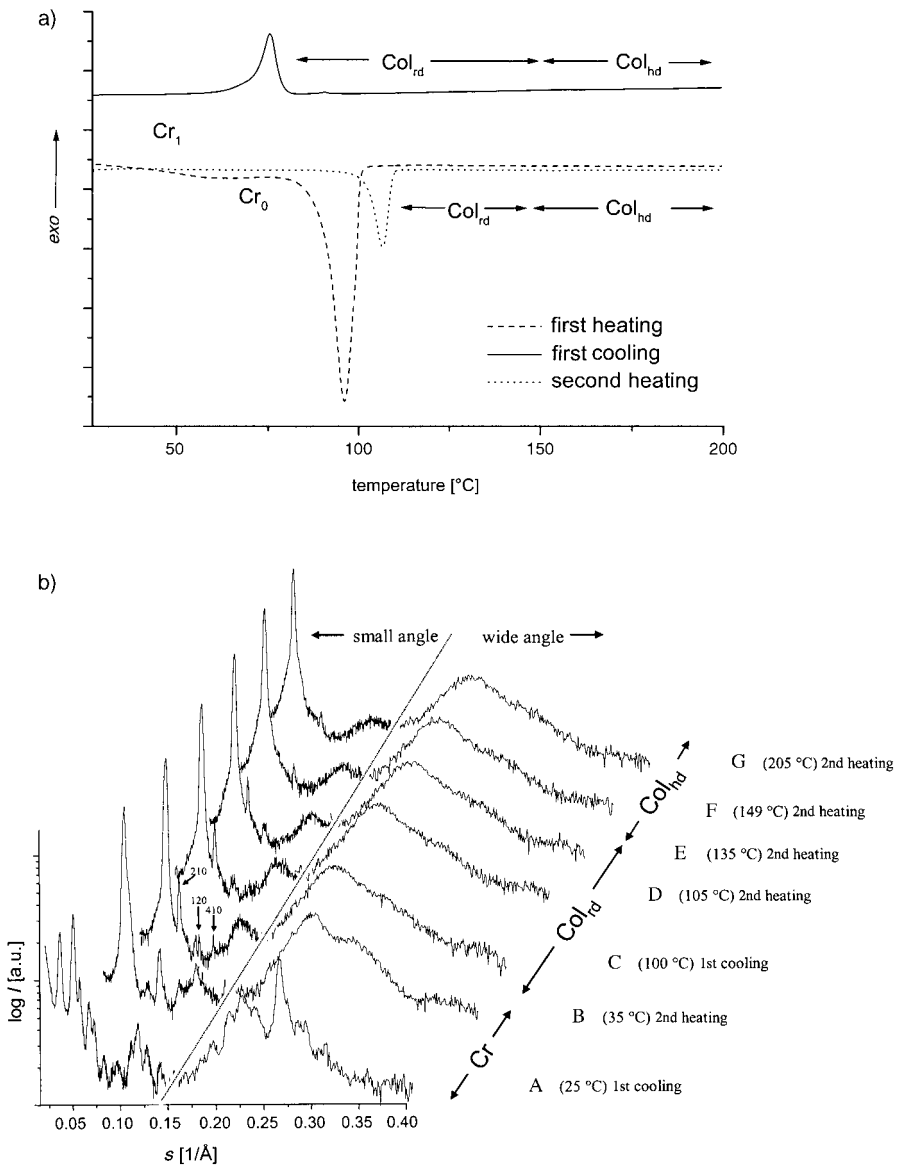

Figure 3. a) DSC traces and b) temperature-dependent synchrotron radiation X-ray powder diffraction patterns of **1d**, both at a heating rate of 10° min^{-1}. The relative X-ray intensity is represented on a logarithmic scale.

*X-ray diffraction of an oriented fibre of **1d***: A small intra-columnar distance between adjacent discotic molecules is essential for efficient charge-transport properties. However, the powder diffraction measurements display neither a reflection at wide angles, normally attributed to a well-defined intra-columnar stacking distance, nor a pronounced shoulder to the halo region, typically attributed to the average distance between disks. A second broad halo, which decreases with increasing temperature, is obtained at about 8.7 Å and has not yet been discussed. To obtain more information on the structure of the mesophase, 2D X-ray studies on samples aligned by extrusion of thin filaments have been carried out. The results obtained are presented in Figure 4. A good alignment of columns along the fibre direction in the rectangular phase at 135 °C (Figure 4a) is demonstrated by the fact that all reflections (200, 110, 210 and 020) related to the rectangular 2D lattice of the columns are located on the equator of the X-ray pattern. The diffuse peak at 8.7 Å can be found on the meridian and is attributed to the disordered stacking of mesogens along the columns.[27] The splitting into four maxima on both sides of the meridian is attributed to a tilt of the disks of ≈23° (structure **C** in Figure 5). The large intra-columnar distance can be explained if nearest neighbours are displaced along the columnar axis. Figure 5 presents two possible explanations for this observation. Adjacent mesogens can be translationally displaced, as depicted in structure **A**, or they can be rotationally displaced (staggered) as illustrated in structure **B**. These two schematic drawings show only extreme situations and a combination of both is most probably present in the LC phase.[28] In either case, the distance between the closest aromatic planes amounts to 4.4 Å. In addition to the equatorial and meridional features, there is a halo with a maximum at 4.5 Å. Its intensity is not circularly distributed, as expected for liquid-like aliphatic chains, but exhibits a set of four, rather intense diffuse maxima at an angle of 60° with respect to the meridian. These results can be explained if aliphatic chains are partially oriented and tilted by approximately 37° relative to the aromatic plane.[25] At larger angles, a set of four very diffuse reflections at 3.7 Å is observed. The origin of these features has not been unambiguously established yet; however, the distance is close to the van der Waals distance between sulfur atoms[26] and may be thus related to short-range order of the sulfur atoms at the periphery of the aromatic cores. Figure 4b shows the two-dimensional diffraction pattern of **1d** in its hexagonal phase at 170 °C. Here, no intense signals on the halo related to a preferred orientation of the aliphatic chains can be identified, which implies a more liquid-like organisation of these molecular segments. The splitting of the diffuse signal at 8.7 Å has also disap-

© 2005 Wiley-VCH Verlag GmbH & Co. KGaA, Weinheim

Table 2. Results of temperature-dependent X-ray measurements on powders and oriented fibres.

Compound	Mesophase	*hkl*	d_{exp} [Å]	d_{calcd} [Å]	Lattice parameter [Å]	ρ_{calcd}[c] [g cm^{-3}]
1a	Col_{hd}	100	20.5	–	a = 23.6	1.03
	(220 °C)		4.5 (halo)		c~3.6	
			3.6 (shoulder)			
1b	Col_{hd}	100	21.6	–	a = 25.0	1.04
	(190 °C)		4.7 (halo)		c~3.7	
			3.7 (shoulder)			
1c	X[a]	010	24.4	–	a = 37.6	1.13
	(134 °C)	110	20.0	20.5	b = 24.4	
		200	18.8	–	c = 9.1[b]	
		020	12.4	12.2		
		300		12.5		
		230	9.1	8.7		
		001	9.1[b]	–		
		201	8.2[b]	8.2		
		211	7.7[b]	7.7		
			4.6 (halo)			
	Col_{rd1}[a]	200	22.3	–	a = 44.6	1.00
	(170 °C)	110	21.2	–	b = 24.1	
		210	16.3	16.4	c~8.7[b]	
		001	8.1 (split)			
			4.6 (halo)			
	Col_{rd2}[a]	200	22.7	–	a = 45.5	0.91
	(210 °C)	110	22.7	–	b = 26.2	
		210	17.2	17.2	c~8.7[b]	
			8.1 (diffuse)	–		
			4.7 (halo)			
	Col_{hd}	100	23.0		a = 26.6	0.92
	(225 °C)		8.4		c~8.4	
1d	Col_{rd}	200	23.2	23.7	a = 46.4	0.87
	(100 °C)	110	23.2	23.2	b = 27.6	
		210	17.8	17.8	c~9.5[b]	
		020	13.7	13.8		
		120	13.1	13.2		
		410	10.8	10.7		
		001	8.7 (split)	–		
			4.6 (halo)	–		
	Col_{hd}	100	24.7	–	a = 28.5	0.91
	(165 °C)	110	14.3	14.3	c~8.2	
			8.2	–		
			4.6 (halo)			

[a] Data from measurements with a θ/θ diffractometer. [b] Intracolumnar distances assigned by means of measurements on oriented fibres, taking into account the tilt of the mesogens. [c] Density calculated with $r = Z \times M/(N_A \times V_{unit\ cell})$; Z number of molecules in the unit cell, M Molecular weight and N_A Avogadro constant.

peared, thus indicating that the mesogens are no longer tilted with respect to the columnar axis in the Col_{hd} phase.

*X-ray diffraction of compound **1c***: Results similar to **1d** have been obtained for molecule **1c** (Figure 6). After synthesis, a Cr_0 phase is formed.[23] Although relatively intense signals at 3.89 Å and 3.81 Å (Figure 6b) are observed,[24] the reflection at 3.5 Å is attributed to regular π-stacking. As in the case of **1d**,[23] oriented samples of **1c** could not be obtained in the Cr_0 phase because the latter is not recovered after heating to 210 °C and subsequent cooling to room temperature. After the Cr_0 phase melts at 95 °C, a Cr_1 phase has partially formed (Figure 6a, first heating). The Cr_1 phase is not fluid, although the broad halo and the absence of other reflections in the wide-angle region indicates disorder of the aliphatic chains (Figure 6b, pattern B). At 116 °C, a mesophase X is generated, which is waxy and can be sheared between glass plates. This phase has been additionally studied with a θ,θ-diffractometer (Figure 7b). Columns are arranged on a primitive rectangular lattice, which is determined by six reflections in the small-angle range (Table 2). Because only a halo corresponding to liquid-like aliphatic chains is observed at wide angles, it was suggested that this phase has a LC character. However, the investigation of an oriented fibre reveals three rather sharp reflections at medium angles, which are related to order along the columns (Figure 7b). Two of them are reflections with mixed indices *hkl*, indicating the crystalline nature of the phase. The third reflection is indexed as 001 and displays a periodicity of 9.1 Å along the columns. As for **1d** in its Col_{rd} phase, the closest mesogens **1c** are distinguished by means of X-ray studies, and the distance between nearest neighbours amounts to 4.5 Å. Despite the three-dimensional order of the aromatic cores, the waxy consistency of the material points to an anisotropic plastic crystalline phase.[29] When heated above the transition temperature of 134 °C, a rectangular LC phase forms. Previously, the mesophase between 134 and 181 °C was indexed according to an oblique phase.[17] In principle, oblique or rectangular symmetry may explain the three reflections at small angles found in the powder pattern (Figure 6 and Table 2). However, since the unit cell is clearly primitive rectangular for derivative **1d**, which has only two more methylene units per chain, we reassign this mesophase to a rectangular, primitive organisation of columns. The study of oriented fibres shows a splitting of the diffuse signal at 8.1 Å into a set of four reflections along the meridian and indicates that molecules are tilted by approximately 22° in the Col_{rd1} phase. It should be noted that, although there is a difference in structure between the X and Col_{rd1} phases, the small thermal hysteresis of only 6 °C and the low enthalpy change of 1.6 kJ mol^{-1} demonstrates the intermediate nature of X between a crystal and a liquid crystal (Col_{rd}). The cell parameters of the Col_{rd} phase only change gradually with tempera-

 © 2005 Wiley-VCH Verlag GmbH & Co. KGaA, Weinheim

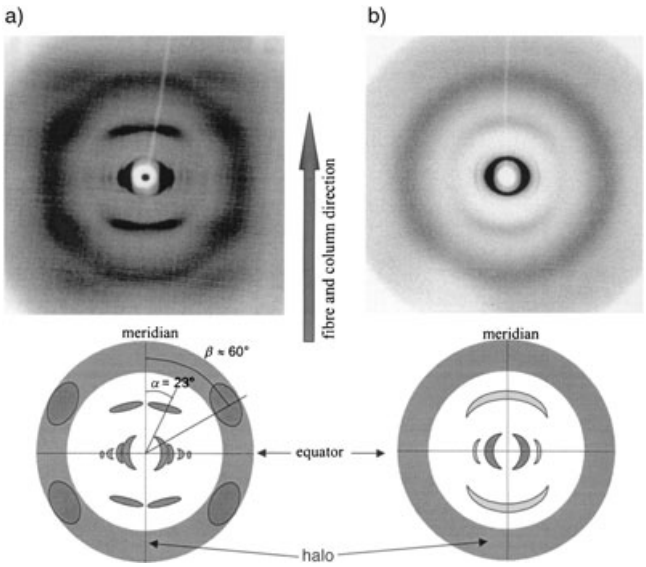

Figure 4. X-ray diffraction patterns (above) and schematic drawings (below) of oriented fibres of **1d**. a) At 135 °C in the Col_{rd} phase and b) at 170 °C in the Col_{hd} phase. Fibres were prepared by extrusion at 200 °C.

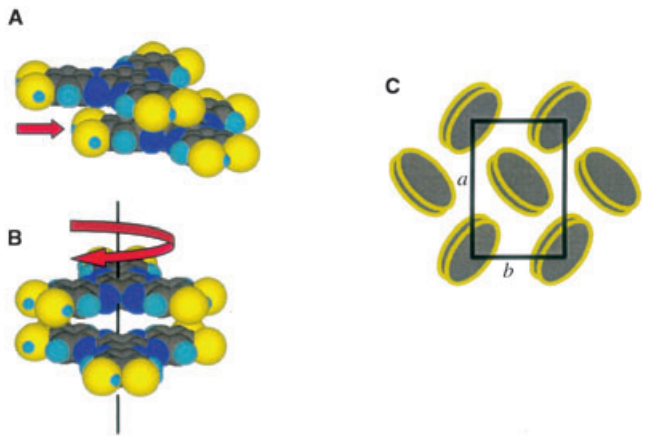

Figure 5. Possible assembly of discotic HATNA mesogens in the rectangular columnar mesophase. Alkyl chains are omitted for reason of clarity. The mesogens could be translationally (**A**) or rotationally displaced (**B**) with respect to adjacent molecules. Structure **C** illustrates the packing of the columns in a rectangular non-centred lattice. The elliptic cross-section of the columns indicate the inclination of mesogens with respect to the columnar axis.

ture. Although a small transition occurs at 181 °C (0.3 kJ mol^{-1}) in the DSC curves, no discontinuous structural changes have been detected by powder diffraction (Figure 6). With increasing temperature, the reflection at 8.1 Å becomes more diffuse and the splitting disappears. At 222 °C, only one main reflection is observed at 23 Å, which can, in principal, be attributed to a lamellar columnar or a hexagonal columnar phase. Interestingly, similarly to **1d**, no peak in the DSC is observed at the transition (≈222 °C) to the high-temperature mesophase. By analogy to **1d**, the high-temperature mesophase of **1c** could be a hexagonal phase, although a 110 reflection is not present. Owing to the decomposition of the molecules before the clearing, no typical texture has been obtained that could help to distinguish between hexagonal and lamellar assemblies.

*X-ray diffraction of **1a** and **1b***: X-ray patterns in the LC phases of the two smallest molecules, **1a** and **1b**, show only one reflection (Figure 8a, patterns C and D, as well as Figure 8b, patterns D and E) and, as is the case for **1c**, no unambiguous structural assignment can be made. The absence of a diffuse signal at about 8.7 Å and the more pronounced shoulder of the halo between 3.5–3.7 Å for **1a** and **1b** in their LC phases indicate that adjacent molecules cannot be distinguished within the columns by X-ray investigations. This is probably caused by the relatively faster dynamics of the molecules compared to the derivatives **1c** and **1d** with longer chains. However, the small inter-molecular distance of 3.5–3.7 Å compared to 4.1 Å in **1c** and **1d** seems to be unreliable and could be an effect of overlapping intensities originating from π stacks and from short-range correlations between sulfur atoms, as discussed for the 2D X-ray pattern of **1d**. At lower temperatures, the two compounds form crystalline phases. As already mentioned, **1a** is obtained in one principal crystal modification after synthesis. Additional minor reflections in the powder pattern of the untreated material show that there is a small amount of at least one other metastable crystal modification (Figure 8a, pattern A). After the first heating phase, these reflections disappear and only Cr_1 is present (Figure 8a, pattern C). X-ray studies of oriented fibres reveal a periodicity of 9.4 Å along the fibre axis.[30] The unit cell is body-centred because only reflections following the rule $h + k + l = 2n$ are observed, thus rationalizing that only the 002 reflection appears on the meridian. In contrast to diffraction patterns obtained in the LC phases of **1c** and **1d**, where the set of four reflections in the range of 8–9 Å indicates a tilt of the mesogens, a similar pattern observed for **1a** corresponds to the mixed reflections 202 and 022. The mesogens of adjacent columns would be shifted by $c/2$ to form a body centred unit cell containing four molecules. Compound **1b** shows a more complex behaviour in its crystal phases at low temperature as also revealed by DSC studies. X-ray analysis indicates a transformation from the Cr_0 to the Cr_1 phase at 150 °C in the first heating phase. The pattern of Cr_0 (Figure 8a, pattern A) shows a signal at 3.8 Å, and additional reflections at wide angles, which could be related to a regular π-stacking, have not been detected. In the Cr_1 phase at 160 °C (Figure 8a, pattern B), the reflection at 3.8 Å has disappeared. The broad halo relates to relatively disordered alkyl chains. However, at small angles, there is a series of relatively sharp reflections that accounts for the crystalline character of the phase.[30]

As discussed before, the structures of the high-temperature mesophases of **1a**--**1c** could not be unequivocally established owing to the presence of only one reflection at small angles. However, experimental Bragg distances (d_{exp}) and calculated parameters a of a hexagonal phase can be compared to estimated diameters d_{col} of the mesogens in the columns. For a lamellar phase, these diameters should be close

© 2005 Wiley-VCH Verlag GmbH & Co. KGaA, Weinheim

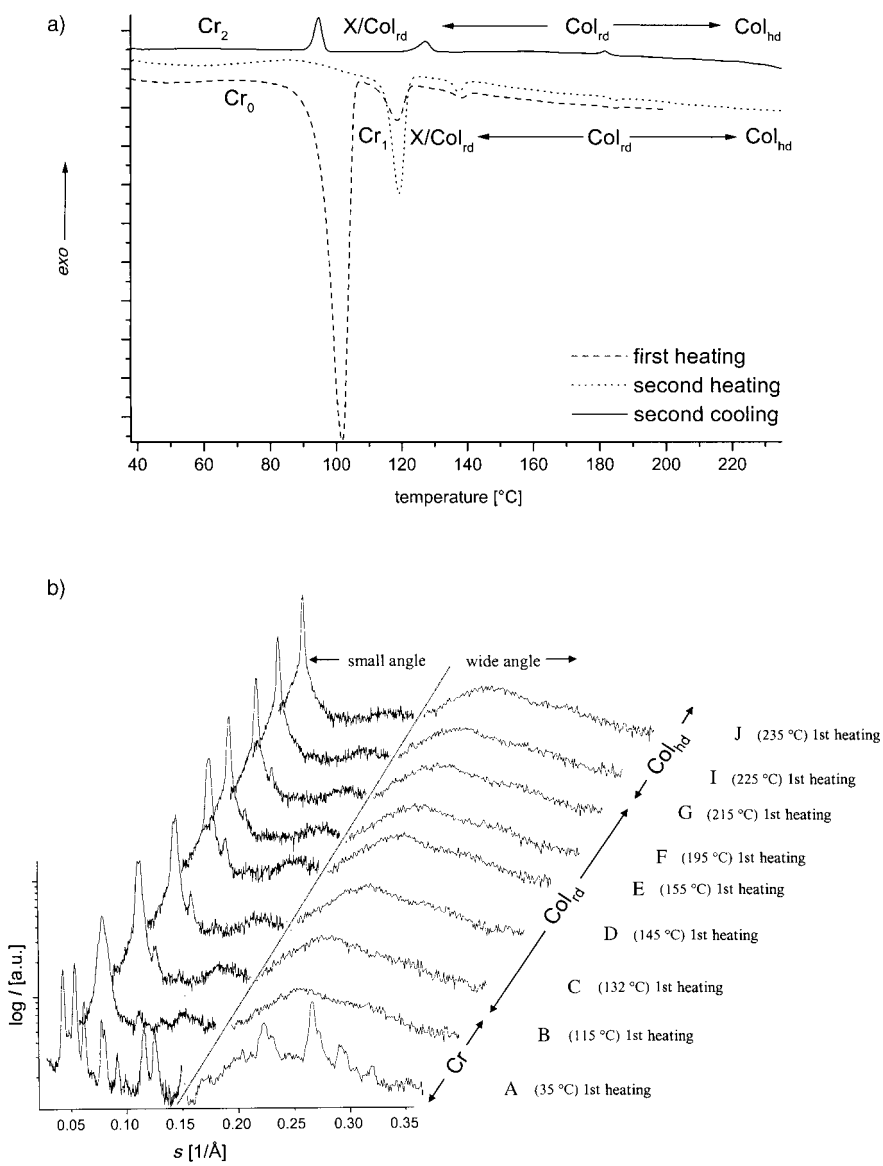

Figure 6. a) DSC traces and b) temperature-dependent synchrotron radiation X-ray powder diffraction patterns of **1c**, both at a heating rate of 10°min^{-1}. The relative X-ray intensity is represented on a logarithmic scale.

to the d_{exp} values, whereas for hexagonal columnar phases, they should approach the a parameters. On the basis of a model with segregated aliphatic chains uniformly surrounding a rigid aromatic core, the columnar diameter d_{col} can be estimated from the volume fraction occupied by the CH_2 groups,[31] the thickness of a columnar slice h_{col}, and the radius of the HATNA core derived from a molecular model. The height h_{col} is estimated to be 4.1 Å for all phases, although shoulders at smaller spacings have been detected. This is rationalised by the uncertainty of the reflection maximum caused by overlap with the halo and by the lack of a clearly identified origin of the diffuse scattering in this range (since for the rectangular phase of **1d** the diffuse scattering at 3.7 Å does not seem to be related to the π stacks).

The results for the high-temperature mesophases above 200°C are collected in Table 3. The estimated columnar diameters d_{col} are 4–5 Å larger than d_{exp} values, but deviate only by 1–2 Å from the a parameters of a hexagonal unit cell. The remaining discrepancy between parameters a and d_{col} can be explained by two factors: 1) the non-circular shape of the aromatic core, which implies that the unoccupied space between the branches of the C_3-symmetric mesogen could be partially occupied by the lateral alkyl chains, 2) the experimental error for d_{exp} and h_{col}, which are estimated to ±0.2 Å and ±0.5 Å, respectively. The latter is more pronounced because there is only a diffuse signal associated with the intra-columnar distance. Overall, the results point to a hexagonal structure for the high-temperature mesophases.

Charge-carrier mobility: The conducting properties of compounds **1a**–**1d** have been studied by means of the pulse-radiolysis time-resolved microwave-conductivity technique.[32,33,34] Transient changes in the conductivity of the freshly precipitated samples are shown in Figure 9. The temporal form and magnitude of the transients differ dramatically: from barely detectable for **1a** to large and long-lived for **1c**. Compounds **1b** and **1d** display intermediate behaviour with evidence for a short-lived component that decays within the pulse followed by a slower after-pulse decay. Mobilities have been estimated from the end-of-pulse value of the slowly decaying components for **1b**, **1c** and **1d**, and these are plotted as a function of temperature in Figure 10.

For all three compounds $\Sigma\mu_{1D}$, the sum of the hole and electron mobilities, is found to increase gradually with increasing temperature on the first heating run, up to a temperature close to the first phase transition observed in the DSC and temperature-dependent X-ray scans. Above this temperature, an abrupt decrease in mobility occurs to a value which remains almost constant on further heating to the maximum temperature achievable by our setup, namely

 © 2005 Wiley-VCH Verlag GmbH & Co. KGaA, Weinheim

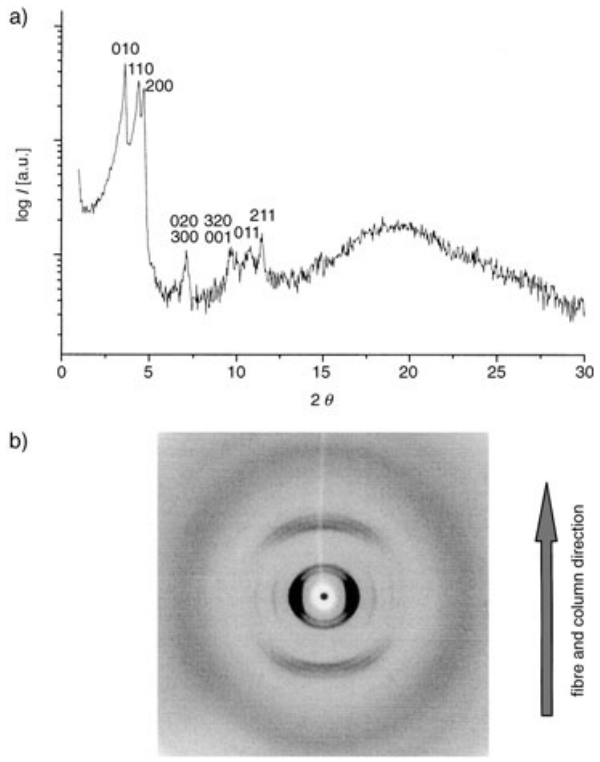

Figure 7. a) X-ray powder diffraction patterns of **1c** at 134 °C (Siemens D500 Kristalloflex, θ/θ-goniometer) and b) 2D X-ray pattern obtained with an extruded fibre at 130 °C. The reflections with low intensity at medium angles determine the order along the *c* axis.

Table 3. Comparison of experimental values, d_{exp} and a, with columnar diameter d_{col} estimated by considering the specific volumes V_{CH_2}, V_{core} for the high temperature mesophase.

Compound	T[°C]	V_{CH_2}[a]	d_{col}[Å][b]	d_{exp}[Å]	a[Å][c]
1a	220	1115	24.2	20.5	23.6
1b	200	1467	26.4	22.2	25.6
1c	225	1864	28.6	23.0	26.6
1d	205	2208	30.4	25.5	29.5

[a] V_{CH_2} is the volume fraction occupied by methylene groups, estimated by $V_{CH_2} = 26.56 + 0.02\,T$ [T°C].[31] [b] The columnar diameter was estimated by $d_{col} = 2\times r_{col}$; r_{col} is derived from $r_{col} = \sqrt{(V_{CH_2}/(\pi\times h_{col}) + r^2_{core})}$; h_{col} is the average distance of mesogens along a column and is estimated to 4.1 Å; r_{core} is the radius of the aromatic centre, $r_{core} = 7.75$ Å. [c] a is the cell parameter of a hypothetical hexagonal unit cell calculated from experimental data by $a = 2\times d_{exp}/\sqrt{3}$.

200 °C. Upon transition from the crystalline to the liquid-crystalline phase, the side chains become more liquid-like, and this "melting" of the side chains reduces the efficiency of charge transfer between neighbouring hexaazatrinaphthylene cores within the columnar stack on account of increased molecular disorder. A common feature of a number of different discotic materials is the decrease of mobility upon phase transition from the crystalline to the liquid crystalline structure, and it remains relatively constant throughout the liquid crystalline phase.[6] Table 4 gives the values of $\Sigma\mu_{1D}$ at room temperature, just below the transition temperature and in the columnar phase at the indicated temperature T. The difference in the absolute magnitudes of the mobilities on changing the length of the peripheral alkyl chains, particularly in the crystalline phases of the present compounds, is not characteristic of other large aromatic discotics, such as phthalocyanines[33] or hexabenzocoronenes;[6] for such compounds, the temperature dependences and absolute values of $\Sigma\mu_{1D}$ were found to be only moderately dependent on the chain length. The large differences observed for the present materials can be rationalised by the different morphologies of the crystals after preparation. The mobility of charges depends critically on the overlap of the frontier orbitals in the crystal or in the liquid crystal.[11,16] Precise structural information necessary for accurate theoretical calculations is not available for these compounds because single crystals of sufficient quality could not be obtained. Figure 3 and Figure 6 exhibit reflections at approximately 3.5 Å in the crystal phases of **1c** and **1d** that may be attributed to a π-stacking distance. These disappear on entering the LC phase. The charge-carrier mobility decreases concurrently with the structural change. While this 3.5 Å reflection has not been observed in **1b**, the high charge-carrier mobility suggests a similar π stacking as for the crystal structures Cr_0 of **1c** and **1d**. In contrast, **1a** shows a very low charge-carrier mobility in the Cr_1 phase, which may be explained by insufficient overlap of the aromatic cores of adjacent molecules in the body-centred unit cell.[19]

Table 4. The one-dimensional charge-carrier mobilities, $\Sigma\mu_{1D}$ [$cm^2V^{-1}s^{-1}$], for the first heating and cooling cycle at room temperature, at the temperature of maximum mobility in the crystalline phase, in the columnar mesophase and on returning to room temperature. The final column gives the mobility at 180 °C after a second heating phase.

Compound	1st heating μ(RT)	1st heating $\mu_{max}[T]$ [$cm^2V^{-1}s^{-1}$]	1st heating $\mu_{LC}[T]$ [$cm^2V^{-1}s^{-1}$]	1st cooling μ(RT) [$cm^2V^{-1}s^{-1}$]	2nd heating μ(180 °C)
1a	<0.01	–	–	–	–
1b	0.07	0.29 (160 °C)	0.05 (180 °C)	0.10	0.07
1c	0.59	0.87 (85 °C)	0.26 (180 °C)	0.13	0.32
1d	0.27	0.28 (40 °C)	0.02 (110 °C)	0.04	–

As can be seen in Figure 10, only in compound **1b** does the mobility return close to the same trajectory on cooling. In the cases of **1c** and **1d**, there is no indication of a return to the initial crystalline phase with the higher mobility. This is in agreement with the DSC and X-ray data that indicate the absence of the initial crystal phase Cr_0 and the reflection at approximately 3.5 Å for **1c** and **1d** upon cooling. Compound **1b** returns reversibly to its Cr_1 phase at high temperature, but not to the initial crystal Cr_0, which is evidenced by DSC traces. The phases Cr_2 and Cr_1 of **1b** still show mobilities similar to the virgin material. For all three compounds, the second heating trajectory closely follows the data obtained on cooling and the values of $\Sigma\mu_{1D}$ at high temperatures are reproduced within the limits of experimental error.

Because the mobility is dependent on intracolumnar order and less on the intercolumnar ordering,[6,35] the mobili-

© 2005 Wiley-VCH Verlag GmbH & Co. KGaA, Weinheim

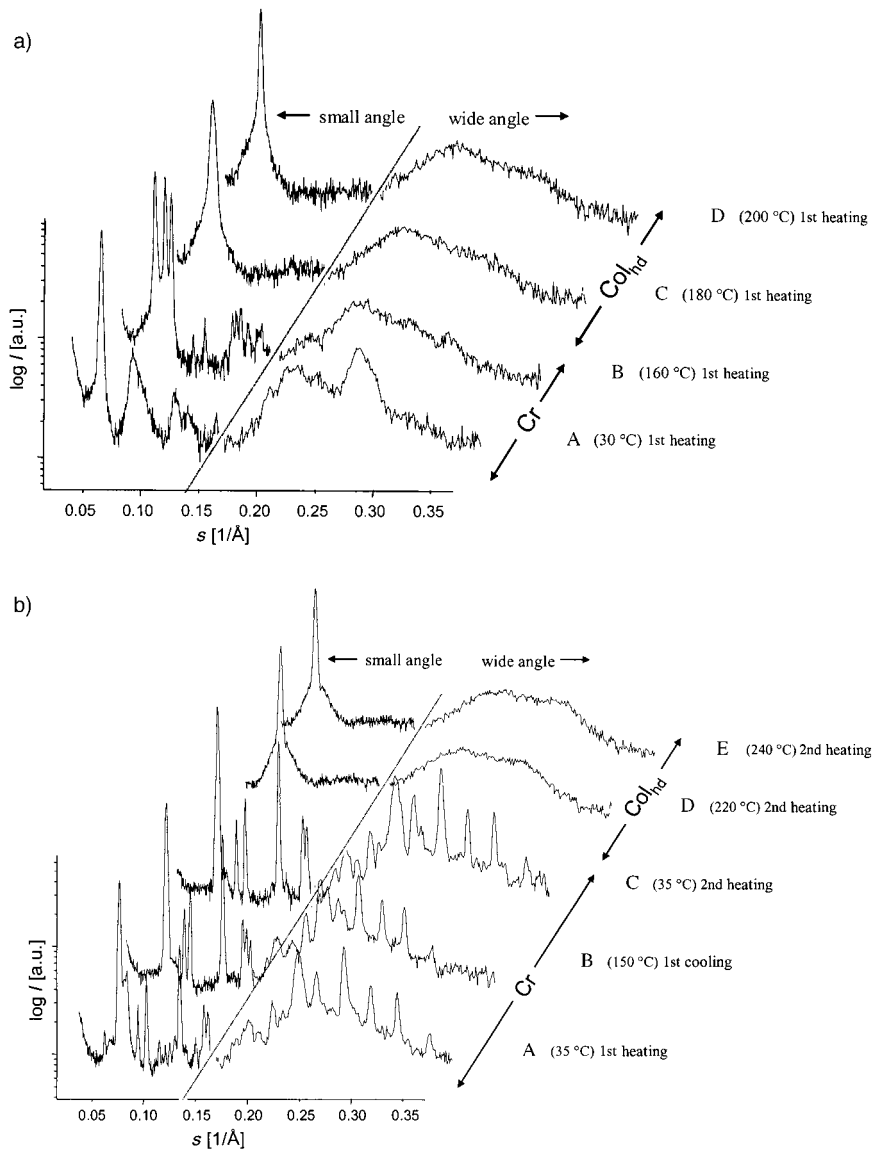

Figure 8. Temperature-dependent synchrotron radiation X-ray powder diffraction patterns of a) **1b** and b) **1a** measured at a heating rate of 10° min^{-1}. The relative X-ray intensity is represented on a logarithmic scale.

ties in the mesophase are relatively temperature-independent, despite rearrangements of the column ordering (from rectangular to hexagonal packing, for example). The source of the higher mobility in the liquid-crystalline phases of **1c**, as compared to the other compounds, is not immediately apparent from the X-ray data. The structure in the Col$_{rd1}$ phase of **1c** is quite similar to the Col$_{rd}$ phase of **1d** (see Table 2). However, the mobility value in the latter is approximately one order of magnitude lower. X-ray diffraction of LC phases can determine the overall symmetry of columnar organisation and average intracolumnar distances between aromatic mesogens. However, for the present HATNA molecules, more detailed information on the supramolecular assembly along the columns is necessary to correlate the charge transport and the structural data. Obviously, the alkyl chains have a large impact on the π stacking of the aromatic mesogens, and thus on the charge-carrier mobility. The mobilities determined for the HATNA derivatives in the mesophase described in this work are higher than the mesophase mobilities ($\Sigma\mu_{1D} < 0.01$ cm^2 V^{-1}s^{-1}) found for the similar hexakis-(hexylthio)triphenyene.[6,36]

Conclusion

Hexaazatriphenylenes derivatives with an electron-deficient core containing six nitrogen atoms and substituted by six electron-donating alkylsulfanyl chains at the periphery, have been designed to efficiently transport electrons. The molecules possess a low reduction potential of −1.09 V. The aliphatic side-chains induce liquid crystalline phases. Mesogens with the shortest chains (hexyl and octyl) show only one mesophase (Col$_{hd}$) at high temperatures. Mesogens with longer chains (decyl and dodecyl) form columnar mesophases of lower symmetry (Col$_{rd}$) at lower temperatures and even an anisotropic plastic phase has been found as an intermediate state between the crystal and liquid crystal phases for **1c**. Along the columns, mesogens do not pack in an eclipsed conformation; it can be thus assumed that adjacent molecules are rotationally or translationally displaced. There is a significant variability of the measured LC phase mobilities (from 0.02 to 0.32 cm^2 V^{-1}s^{-1}) with changes in the side-chain length. Apparently, the side-chains have a strong influence on the intracolumnar ordering of these molecules. This contrasts with the results of studies on larger discotic molecules, such as hexabenzocoronenes,[6] for which the mobilities in the LC phase are found to be primarily independent of the side-chains. The LC mobilities in the hexabenzocoronenes have the same order of magnitude as those found in the present compounds (~0.3 cm^2 V^{-1}s^{-1}).

In summary, the HATNA molecules emerge as promising semiconductors owing to their high charge-carrier mobilities. The core is electron-deficient and should facilitate electron injection, thus making these compounds good electron transporters. However, transition temperatures are currently too

 © 2005 Wiley-VCH Verlag GmbH & Co. KGaA, Weinheim

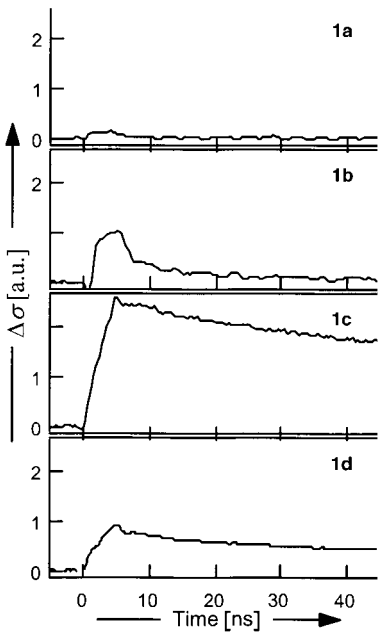

Figure 9. Room-temperature microwave conductivity transients of freshly precipitated samples of **1a**, **1b**, **1c** and **1d** with 2 ns (**1c**) or 5 ns (**1a**, **1b**, **1d**) electron pulses.

high for practical use. Work is in progress to lower the melting and clearing temperatures in order to obtain LC phases at room temperature and an isotropic phase below 200 °C.

Experimental Section

Solvents and reagents were purchased from Aldrich and used as received. Column chromatography was performed on silica gel (Merck silica gel 60, mesh size: 0.2–0.5 mm). ^{1}H NMR spectra were recorded in $CDCl_3$ as the solvent on a Bruker Avance 300 with the solvent signal as the internal standard. Mass spectra were recorded on a VG Micromass 7070F instrument (electron impact, 70 eV) and a VG analytical ZAB 2-SE-FPD: FD (8 kV). Elemental analysis was carried out at the microanalytical laboratory of the University of Mainz (Germany). The thermal behaviour of all the materials synthesised was investigated by polarising optical microscopy (JENA microscope equipped with a Mettler FP 52 hot stage) and differential scanning calorimetry (Mettler Toledo DSC 821, 3–9 mg samples in closed Al pans) with heating and cooling scans performed at ramping rates of 10 °C min^{-1}. Powder X-ray diffraction measurements were performed on the X33 camera of the European Molecular Biology Laboratory at the storage ring DORIS III of the Deutsches Elektronen Synchrotron (DESY), Hamburg (Germany). Diffraction patterns were collected in transmission in series of frames of 10 s or 6 s each with two-position sensitive delay line readout detectors connected in series.[37,38] The sample temperature was controlled with a Mettler FP-82 HT heating stage under a nitrogen flux. The data were normalised to the intensity of the primary beam with the SAPOKO program.[39] The modulus of the scattering vector ($s = 2\sin\theta/\lambda$, where 2θ is the Bragg angle and λ the wavelength (1.5 Å)) was calibrated with tripalmitin and/or rat tail collagen in the small s region and benzoic acid in the high s region. The X-ray powder diffraction patterns of **1c** at 134 °C were recorded on a Siemens D 500 Kristalloflex with a graphite-monochromatised $Cu_{K\alpha}$ X-ray beam emitted from a Rigaku RV-300 rotating anode source. The temperature of the sample on the copper sample holder was monitored with a bimetal sensor, previously calibrated by reference measurements. The WAXS measurements on aligned samples obtained by extrusion at 220 °C were made with a rotating anode (Rigaku 18 kW) source with pinhole collimation equipped with a graphite double monochromator (λ = 0.154 nm) and a Siemens area detector with 1024 × 1024 pixels. The beam diameter was ≈0.5 mm and the sample-to-detector distance was 80 mm. Measurements were performed on cylindrical filaments with a thickness of 0.7 mm. The patterns were recorded with vertical orientation of the filament axis and with the beam perpendicular to the filament.

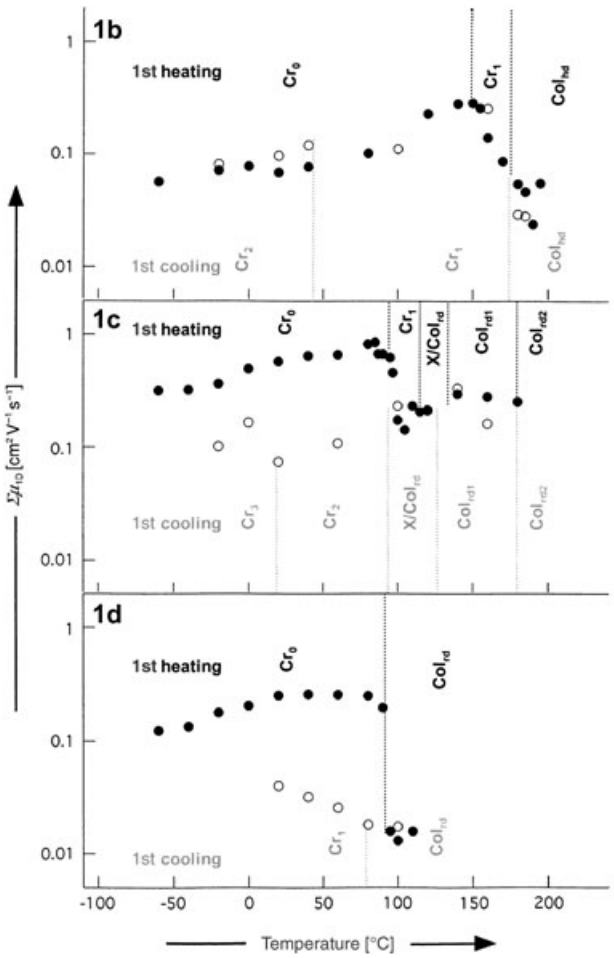

Figure 10. One-dimensional, intracolumnar charge-carrier mobilities ($\Sigma\mu_{1D}$) as a function of temperature for **1b**, **1c** and **1d** for the first heating (●) and cooling (○) trajectories. The vertical arrows indicate the temperatures at which a peak appears in the DSC measurements (see Table 1).

The cyclic voltammetry studies were carried out in dichloromethane solution of compounds **1** (10^{-4}–10^{-3} M). Tetra-*n*-butylammonium perchlorate was used as the supporting electrolyte in a conventional three-compartment cell, equipped with a glassy carbon, SCE and platinum wire as working, reference and auxiliary electrodes, respectively. Measurements were carried out under an inert atmosphere with an Autolab (Eco Chemie) PGSTAT 30 potentiostat with a Scan-Gen module at a scan rate of typically 200 mV s^{-1}.

The pulse-radiolysis time-resolved microwave-conductivity technique and method of data analysis as applied to discotic materials have been previously described in detail.[33,34] Briefly, solid samples in the form of powders are compressed into a Ka-band (≈30 GHz) microwave cell. Uniform micromolar concentrations of charge carriers are produced in the sample by a 2—50 nanosecond pulse of 3 MeV electrons from a van de Graaff accelerator. This method of ionisation has the advantage that it does not perturb the primary or higher order molecular structure of the

© 2005 Wiley-VCH Verlag GmbH & Co. KGaA, Weinheim

material, as is the case for other procedures, such as chemical doping.[40] The amount of energy deposited in the sample, $DJ\,m^{-3}$, is accurately known from dosimetry and the beam charge in the pulse which is routinely measured. If the charge carriers are mobile, microwaves propagating through the sample are attenuated and this is monitored as a reduction in the microwave power reflected by the cell on irradiation. The change in conductivity, $\Delta\sigma/D$, is derived from the change in microwave power, $\Delta P/P$, using the known sensitivity factor A [Eq. (1)].

$$\frac{\Delta P}{P} = -A\Delta\sigma \tag{1}$$

If the lifetime of the charge carriers is much longer than the pulse width, the sum of the one-dimensional, intracolumnar mobilities, $\Sigma\mu_{1D}$, can be calculated from the dose-normalised end-of-pulse conductivity according to Equation (2).

$$\sum\mu_{1D} = \frac{3\,E_P[\Delta\sigma_{eop}/D]}{W_{eop}} \tag{2}$$

Where E_p is the average energy absorbed in electron volts per initial ionisation event, which is taken to be ≈ 25 eV for the present materials.[41,42] W_{eop} is the probability that the initially formed electrons and holes become localised on separate columnar stacks and do not decay within the pulse. The values of W_{eop}, calculated as described previously,[33] were 0.39, 0.47, 0.49 and 0.51 for **1a**, **1b**, **1c** and **1d**, respectively. A factor of 3 is included in Equation (2) to take account of the random orientation of the columnar stacks in the samples studied. Whereas the values for the absolute mobilities are subject to error ($\pm 25\,\%$), the relative values are expected to be highly accurate.

General procedure for the synthesis of 1: Potassium carbonate (61.5 mmol) and an excess of 1-alkylthiol (20.6 mmol) were added to a solution of hexachlorodiquinoxalino phenazine[17] (1.7 mmol) in *N,N*-dimethylformamide (100 mL). This solution was heated at 85 °C and stirred for four days under nitrogen. The reaction mixture was then poured into a large volume of water and neutralised with hydrochloric acid. The yellow precipitate was filtered and washed with copious amounts of water. The crude orange material was purified as indicated below.

2,3,8,9,14,15-Hexahexylsulfanyl-5,6,11,12,17,18-hexaazatrinaphthylene (1a): The crude solid was purified by column chromatography (silica, $CHCl_3$/hexane, gradient from 0:10 to 6:4), and the solvent was evaporated to give 1.30 g (1.2 mmol) of a yellow solid. Yield: 69.9 %; ^{1}H NMR (300 MHz, $CDCl_3$): δ = 0.95 (t, 18 H; CH_3), 1.40 (m, 24 H; CH_2), 1.59 (m, 12 H; CH_2), 1.89 (q, 12 H; CH_2), 3.23 (t, 12 H; SCH_2), 8.21 ppm (s, 6 H; arom. CH); ^{13}C NMR (75 MHz, $CDCl_3$): δ = 144.4, 142.4, 141.5, 123.18 (arom. C), 33.2, 31.4, 28.9, 28.1, 22.6, 14.0 ppm (aliph. C); FD-MS: m/z (%): 1083 (80/$[M+2H]^+$), 540 (100$[M]^{2+}$); elemental analysis calcd (%) for $C_{60}H_{84}N_6S_6$: C 66.62, H 7.83, N 7.77; found: C 66.91, H 8.00, N 7.66.

2,3,8,9,14,15-Hexaoctylsulfanyl-5,6,11,12,17,18-hexaazatrinaphthylene (1b): Two consecutive crystallisations from ethanol/toluene and hexane/toluene afforded 137 mg (0.11 mmol) of a yellow solid. Yield 67 %; ^{1}H NMR (300 MHz, $CDCl_3$): δ = 0.91 (t, 18 H; CH_3), 1.32 (m, 48 H; CH_2), 1.58 (m, 12 H; CH_2), 1.90 (q, 12 H; CH_2), 3.22 (t, 12 H; SCH_2), 8.18 ppm (s, 6 H; arom. CH); ^{13}C NMR (75 MHz, $CDCl_3$): δ = 144.3, 142.4, 141.4, 123.1 (arom. C), 33.2, 31.8, 29.5–29.2, 28.1, 22.6, 14.1 ppm (aliph. C); FD-MS: m/z (%): 1250 (100/$[M+H]^{+\bullet}$); elemental analysis calcd (%) for $C_{72}H_{108}N_6S_6$: C 69.18, H 8.71, N 6.72; found: C 68.85, H 8.57, N 6.67.

2,3,8,9,14,15-Hexadecylsulfanyl-5,6,11,12,17,18-hexaazatrinaphthylene (1c): Two consecutive crystallisations from ethanol/toluene and hexane afforded 467 mg (0.33 mmol) of a brownish solid. Yield 61 %; ^{1}H NMR (300 MHz, $CDCl_3$): δ = 0.89 (t, 18 H; CH_3), 1.30 (m, 72 H; CH_2), 1.59 (m, 12 H; CH_2), 1.92 (m, 12 H; CH_2), 3.23 (t, 12 H; SCH_2), 8.21 ppm (s, 6 H; arom. CH); ^{13}C NMR (75 MHz, $CDCl_3$): δ = 144.4, 142.4, 141.5, 123.2 (arom. C), 33.2, 31.9, 29.6–29.2, 28.1, 22.7, 14.1 ppm (aliph. C); FD-MS: m/z (%): 1418 (100$[M]^{+\bullet}$); elemental analysis calcd (%) for $C_{84}H_{132}N_6S_6$ (%): C 71.13, H 9.38, N 5.93; found: C 71.08, H 9.48, N 5.81.

2,3,8,9,14,15-Hexadodecylsulfanyl-5,6,11,12,17,18-hexaazatrinaphthylene (1d): The crude solid was purified by column chromatography (silica, $CHCl_3$/hexane 6:4). After evaporation of the solvent, the solid obtained was purified further by washing the solids with methyl alcohol several times to eliminate the excess of sulfanyl chain. Filtration afforded 1.08 g (0.68 mmol) of a brown solid. Yield 57 %; ^{1}H NMR (300 MHz, $CDCl_3$): δ = 0.88 (t, 18 H; CH_3), 1.28 (m, 96 H; CH_2), 1.61 (m, 12 H; CH_2), 1.90 (m, 12 H; CH_2), 3.24 (t, 12 H; SCH_2), 8.22 ppm (s, 6 H; arom. CH); ^{13}C NMR (75 MHz, $CDCl_3$): δ = 144.5, 142.4, 141.5, 123.2 (arom. C), 33.2, 31.9, 29.7–29.2, 28.1, 22.7, 14.1 ppm (aliph. C); FD-MS: m/z (%): 1586 (100$[M]^{+\bullet}$); elemental analysis calcd (%) for $C_{96}H_{156}N_6S_6$ (%): C 72.67, H 9.91, N 5.30; found: C 72.68, H 9.70, N 5.04.

Acknowledgements

We are grateful to Prof. H. Meier and A. Oehlhof for the completion of the elemental analysis at the University of Mainz and to Prof. P. Heiney for many fruitful discussions. This work was financially supported by the Belgian National Science Foundation (FNRS FRFC No. 2.4560.00), by the Université Libre de Bruxelles, by the Banque National de Belgique, by the Communauté Française de Belgique (ARC No. 00/05-257), and by the European Union (DISCEL G5RD-CT-2000-00321). X-ray (synchrotron) measurements at the EMPL Hamburg were supported by the European Community—Access to Research Infrastructure Action of the Improving Human Potential Programme to the EMBL Hamburg Outstation (HPRI-CT-1999–00017). The work in Mons is partly supported by the Belgian Federal Governement (PAI 5/3), the European Commission within the framework of "Objectif 1: Materia Nova", and project DISCEL, and by FNRS. G.K. and V.L. acknowledge the FRIA for a fellowship. J.C. is an FNRS Research Associate.

[1] For a recent progress report, see: M. O'Neill, S. M. Kelly, *Adv. Mater.* **2003**, *15*, 1135.
[2] I. Seguy, P. Jolinat, P. Destruel, J. Farenc, R. Mamy, H. Bock, J. Ip, T. P. Nguyen, *J. Appl. Phys.* **2001**, *89*, 5442.
[3] G. Lüssem, J. H. Wendorff, *Polym. Adv. Technol.* **1998**, *9*, 443.
[4] L. Schmidt-Mende, A. Fechtenkötter, K. Müllen, E. Moons, R. H. Friend, J. D. MacKenzie, *Science* **2001**, *293*, 1119.
[5] a) D. Adam, P. Schuhmacher, J. Simmerer, L. Häusling, K. Siemmensmeyer, K. H. Etzbach, H. Ringsdorf, D. Haarer, *Nature* **1994**, *371*, 141; b) A. M. van de Craats, J. M. Warman, M. P. de Haas, D. Adam, J. Simmerer, D. Haarer, P. Schuhmacher, *Adv. Mater.* **1996**, *8*, 823.
[6] A. M. van de Craats, J. M. Warman, A. Fechtenkötter, J. D. Brand, M. A. Harbison, K. Müllen, *Adv. Mater.* **1999**, *11*, 1469.
[7] P. Miskiewicz, A. Rybak, J. Jung, I. Glowacki, J. Ulanski, Y. Geerts, M. Watson, K. Müllen, *Synth. Met.* **2003**, *137*, 905.
[8] a) H. Eichhorn, *J. Porphyrins Phthalocyanines* **2000**, *4*, 88–102; b) A. van de Craats, J. M. Warman, *Adv. Mater.* **2001**, *13*, 130.
[9] F. Würthner, *Angew. Chem.* **2001**, *113*, 1069; *Angew. Chem. Int. Ed.* **2001**, *40*, 1037.
[10] D. M. de Leeuw, M. M. J. Simenon, A. R. Brown, R. E. F. Einerhand, *Synth. Met.* **1997**, *87*, 53.
[11] J. Cornil, V. Lemaur, J.-P. Calbert, J.-L. Brédas, *Adv. Mater.* **2002**, *14*, 726.
[12] N. Boden, R. J. Bushby, K. Donovan, Q. Liu, Z. Lu, T. Kreouzis, A. Wood, *Liq. Cryst.* **2001**, *28*, 1739.
[13] I. Seguy, P. Jolinat, P. Destruel, R. Mamy, H. Allouchi, C. Courseille, M. Cotrait, H. Bock, *ChemPhysChem* **2001**, *2*, 448.
[14] a) C. W. Struijk, A. B. Sieval, J. E. J. Dakhorst, M. Van Dijk, P. Kimkes, R. B. M. Koehorst, H. Donker, T. J. Schaafsma, S. J. Picken, A. M. van de Craats, J. M. Warman, H. Zuilhof, E. J. R. Sudhölter, *J. Am. Chem. Soc.* **2000**, *122*, 11 057; b) U. Rohr, C. Kohl, A. M. van de Craats, J. M. Warman, *J. Mater. Chem.* **2001**, *11*, 1789.
[15] a) R. I. Gearba, M. Lehmann, J. Levin, D. A. Ivanov, M. H. J. Koch, J. Baberá, M. G. Debije, J. Piris, Y. H. Geerts, *Adv. Mater.* **2003**, *15*,

 © 2005 Wiley-VCH Verlag GmbH & Co. KGaA, Weinheim

1614; b) H. Bock, A. Babeau, I. Seguy, P. Jolinat, P. Destruel, *ChemPhysChem* **2002**, *3*, 532; c) K. Pieterse, P. A. van Hal, R. Kleppinger, J. A. J. M. Vekemans, R. A. J. Janssen, E. W. Meijer, *Chem. Mater.* **2001**, *13*, 2675.
[16] J. Cornil, D. Beljonne, J.-P. Calbert, J.-L. Brédas, *Adv. Mater.* **2001**, *13*, 1053–1067.
[17] G. Kestemont, V. de Halleux, M. Lehmann, D. A. Ivanov, M. Watson, Y. H. Geerts, *Chem. Commun.* **2001**, 2074.
[18] J. H. R. Tucker, M. Gingras, H. Brand, J.-M. Lehn, *J. Chem. Soc. Perkin Trans. 2* **1997**, 1303–1307.
[19] V. Lemaur, D. A. da Silva Filho, V. Coropceanu, M. Lehmann, Y. Geerts, J. Piris, M. G. Debije, A. M. van de Craats, K. Senthilkumar, L. D. A. Siebbeles, J. M. Warman, J. L. Brédas, J. Cornil, *J. Am. Chem. Soc.* **2004**, *126*, 3271.
[20] S. Janietz, D. D. C. Bradley, M. Grell, C. Giebeler, M. Inbasekaran, E. P. Woo, *Appl. Phys. Lett.* **1998**, *73*, 2453; b) J. L. Brédas, R. Silbey, D. S. Boudreaux, R. R. Chance, *J. Am. Chem. Soc.* **1983**, *105*, 6555.
[21] N. Spielberg, M. Sakar, Z. Luz, R. Poupko, J. Billard, H. Zimmermann, *Liq. Cryst.* **1993**, *15*, 311–330.
[22] J. W. Goodby, G. W. Gray in *Handbook of Liquid Crystals*, *Vol. 1* (Eds.: D. Demus, J. W. Goodby, G. W. Gray, H. W. Spiess, V. Vill), Wiley-VCH, Weinheim **1998**, pp. 17–25.
[23] Information on π stacking, which is closely related to the splitting of the frontier orbitals and hence to charge-carrier mobilities, could be obtained by X-ray diffraction of oriented samples. These samples were produced by extrusion of fibres from LC phases at high temperatures. For untreated crystalline materials (Cr_0), oriented fibres or single crystals could not be prepared. The π–π distances can thus only be estimated from the powder diffraction patterns, considering simultaneously the charge-carrier mobility data in the same phase. The reflection at 3.5 Å cannot be unambiguously related to the π-stacking distance.
[24] H. Kiho, A. Peterlin, P. H. Geil, *J. Polym. Sci. B* **1965**, *3*, 157–160.
[25] A. M. Levelut, *J. Chim. Phys. Phys.-Chim. Biol.* **1983**, *80*, 149.
[26] A. Bondi, *J. Phys. Chem.* **1964**, *68*, 441.
[27] A similar halo was found for polycatenar mesogens in their columnar mesophase, and the authors related the diffuse scattered intensity to an intracolumnar average distance, which corresponds to the height of a "columnar slice", see: B. Donnio, B. Heinrich, H. Allouchi, J. Kain, S. Diele, D. Guillon, D. W. Bruce, *J. Am. Chem. Soc.* **2004**, *126*, 15258–15268.
[28] A group of four reflections is found in columnar liquid crystals when molecules form a helical superstructure; see, for example J. Baberá, E. Cavero, M. Lehmann, J.-L. Serrano, T. Sierra, J. T. Vázquez, *J. Am. Chem. Soc.* **2003**, *125*, 4527–4533, and references therein. The interpretation of the four signals of **1d** resulting from a helical superstructure with a helical pitch of $p = (8.7/\cos 23° \times 3)$ Å = 28.4 Å is qualitatively equivalent to the given model if molecules are regularly rotationally displaced by 60°, thus completing a full helix with six molecules along a column. However, there is no further evidence for such a superstructure.
[29] Preliminary solid-state NMR results studied by Dr. Ingrid Fischbach at the Max-Planck Institute for Polymer Research in Mainz (Germany) confirmed the mobility of the mesogens in the temperature range of the plastic phase.
[30] A table with a possible indexation (**1a**) and 2D diffraction patterns (**1a**, **1b**) are available in the Supporting Information.
[31] M. Marcos, R. Gimenéz, J.-L. Serrano, B. Donnio, B. Heinrich, D. Guillon, *Chem. Eur. J.* **2001**, *7*, 1006–1013.
[32] P. G. Schouten, J. M. Warman, M. P. de Haas, *J. Phys. Chem.* **1993**, *97*, 9863.
[33] P. G. Schouten, J. M. Warman, M. P. de Haas, C. F. van Nostrum, G. H. Gelinck, R. J. Nolte, J. M. Roeland, M. J. Marc, J. W. Zwicker, M. K. Engel, *J. Am. Chem. Soc.* **1994**, *116*, 6880–6894.
[34] J. M. Warman, A. van de Craats, *Mol. Cryst. Liq. Cryst.* **2003**, *396*, 41.
[35] I. Fischbach, T. Pakula, P. Minkin, A. Fechtenkötter, K. Müllen, H. W. Spiess, K. Saalwächter, *J. Phys. Chem. B* **2002**, *106*, 6408–6418.
[36] A. M. van de Craats, M. P. de Haas, J. M. Warman, *Synth. Met.* **1997**, *86*, 2125–2126.
[37] M. H. J. Koch, J. Bordas, *J. Nucl. Instrum. and Methods* **1983**, 208, 461.
[38] G. Rapp, A. Gabriel, M. Dosière, M. H. J. Koch, *Nuclear Instrum. and Methods* **1995**, A357, 178.
[39] P. V. Konarev, V. V. Volkov, A. V. Sokolova, M. H. J. Koch, D. I. Svergun, *J. Appl. Crystallogr.* **2003**, *36*, 1277–1282.
[40] W. J. Pietro, T. J. Marks M. A. Ratner, *J. Am. Chem. Soc.* **1985**, *107*, 5387–5391.
[41] A. Hummel in *The Chemistry of Alkanes and Cycloalkanes* (Eds.: S. Patai, Z. Rappoport), Wiley, New York, **1992**, pp. 743–780.
[42] W. F. Schmidt, A. O. Allen, *J. Phys. Chem.* **1968**, *72*, 3730–3736.

Received: June 9, 2004
Revised: January 6, 2005
Published online: March 30, 2005

© 2005 Wiley-VCH Verlag GmbH & Co. KGaA, Weinheim